macromol

MDPI

Article

Influence of Concentration of Thiol-Substituted Poly(dimethylsiloxane)s on the Properties, Phases, and Swelling Behaviors of Their Crosslinked Disulfides

Danielle M. Beaupre [1], Alexander K. Goroncy [2] and Richard G. Weiss [1,3,*]

[1] Department of Chemistry, Georgetown University, Washington, DC 20057, USA
[2] Department of Chemistry, University of Wyoming, Laramie, WY 82071, USA
[3] Institute for Soft Matter Synthesis and Metrology, Georgetown University, Washington, DC 20057, USA
* Correspondence: weissr@georgetown.edu; Tel.: +1-202-687-6013

Abstract: A simple, efficient procedure has been employed to effect intra- and inter-chain crosslinking of two commercially available thiolated poly(dimethylsiloxane) copolymers (T-PDMS) with 4–6% or 13–17% of mercaptopropyl side-chains. The thiol functional groups were converted to disulfides (D-PDMS) in chloroform solutions of I_2. Importantly, the conditions employed avoid over-oxidation to other types of sulfur-containing species, and the concentration of T-PDMS during the crosslinking reaction dictated the rheological properties and liquid or solid nature of the D-PDMS. The procedure for obtaining the crosslinked copolymers is simpler than other approaches in the literature used to crosslink polysiloxane backbones and to modulate their properties. By changing the concentration of T-PDMS during the treatment with I_2, the degree of intra- and inter-chain crosslinking can be controlled (as assessed qualitatively by the solid or liquid nature of the products and their viscoelastic properties). For each of the T-PDMS materials, there is a concentration threshold, above which products are solids, and below which they are oils. Liquid and solid materials were characterized using ^{1}H and ^{13}C solution-state and ^{13}C solid-state NMR spectroscopy, respectively. They indicate greater than 90% conversion of thiols to disulfides in the presence of excess I_2. The rheological behavior of the liquid products, solvent swelling ability of solid products, and the thermal stability of the reactants and products are described. Furthermore, the solid products exhibit some of the highest swelling values reported in the literature for poly(dimethylsiloxane) (PDMS) materials. As assessed by thermal gravimetric analyses, the disulfide-crosslinked materials are more stable thermally than the corresponding thiols.

Keywords: crosslinking; poly(dimethylsiloxane); thiols; disulfides

Citation: Beaupre, D.M.; Goroncy, A.K.; Weiss, R.G. Influence of Concentration of Thiol-Substituted Poly(dimethylsiloxane)s on the Properties, Phases, and Swelling Behaviors of Their Crosslinked Disulfides. *Macromol* **2023**, *3*, 36–53. https://doi.org/10.3390/macromol3010004

Academic Editor: Ana María Díez-Pascual

Received: 9 December 2022
Revised: 14 January 2023
Accepted: 20 January 2023
Published: 28 January 2023

1. Introduction

Thiols (RSH) and disulfides (RSSR) are naturally present functional components of proteins, biopolymers, and biomolecules. In nature, the interconversion of thiol and disulfides regulates some key biological functions [1]. Additionally, thiol- and/or disulfide-containing polymers have been widely explored as self-healing, stimulus responsive, and biomedical materials due to the ease of converting between the thiol and disulfide forms. Reversible thiol-disulfide exchange and redox pathways are available to thiol- and/or disulfide-containing polymers [2]. These pathways present opportunities for rheologically tunable systems.

Drug delivery is among the most common biomedical applications of thiol- or disulfide-containing polymers [3–5]. Thiol- and/or disulfide-containing polymers have been used for other biomedical applications as well, because they can interact with free thiol side chains in cysteine residues of proteins [6]. The applications of thiol- and disulfide-containing polymers extend beyond biomedicine; dynamic materials, such as self-healing elastomers [7,8], shape memory polymers [9], and stimulus-responsive polymers [10,11] have been designed

as coatings [12], adhesives [13], and sensors [6,14]. Incorporation of thiols and/or disulfides into polymers that contain other stimulus-responsive moieties is an emerging technique that has been used to fabricate multi stimulus-responsive materials that may enhance specificity for both biomedical [11,15,16] and non-biomedical applications [9,14,17].

The reactivity of a disulfide depends on the nature of the R groups flanking the disulfide bond, but there are numerous examples where stimuli such as mechanical stress [18], irradiation with light [19,20], change in solution pH or pKa [21], and addition or removal of electrons [7] have been shown to trigger dynamic exchange between thiol and disulfide forms [1,22]. The ease of thiol oxidation increases from tertiary to primary R groups attached to sulfur. Overall, thiols and disulfides with aryl, primary, or non-aliphatic R groups are favored as self-healing and stimulus-responsive materials, because they are more reactive and dynamic [23,24]. Useful thiol- or disulfide-containing polymers must exhibit strong responses to applied stimuli in the target environment, but they must be stable enough to reach the target environment before they react [6], and aryl disulfides may be too reactive for some applications [1].

This article focuses on the oxidation of primary thiol pendant groups in inexpensive and commercially available poly(dimethylsiloxane) copolymers (T-PDMS; Figure 1). The primary thiol groups of T-PDMS are not as reactive as some thiomers reported in the literature, but they can be crosslinked easily and cleanly using simple redox chemistry. The disulfide-crosslinked products (D-PDMSs) did not demonstrate any discernible reaction when stored in capped vials at room temperature (RT) over the course of >3 years, and exhibited better thermal stability than the corresponding non-crosslinked thiols (T-PDMSs). To the best of our knowledge, the oxidation of primary thiol groups to disulfides in polymers of these co-monomers has not been previously reported. Tamanoi, Nakamura, and coworkers [25,26], synthesized disulfide-containing nanoparticles by hydrolysis of silanes containing 3-mercaptopropyl pendant groups. Structurally, crosslinking in the silane-based nanoparticles was due to the formation of Si-O-Si and disulfide bonds during synthesis, resulting in highly branched networks. Nanoparticles were only degraded in solutions containing a disulfide, glutathione, suggesting that the primary aliphatic disulfide bonds were stable in the absence of a specific trigger.

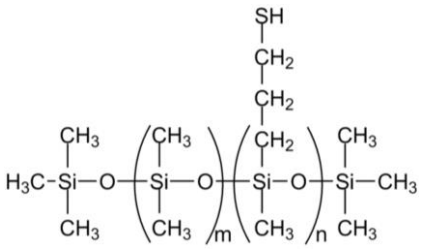

Figure 1. Structure of thiolated poly(dimethylsiloxane) copolymer (T-PDMS). The number of thiol groups per chain, n, is based on the mass average molar weight (M_w) and the percentage of thiol in the T-PDMS. 4–6% T-PDMS has a M_w range of 6000–8000 Da, which corresponds to ranges of m and n values: m = 71–94, n = 3–6. 13–17% T-PDMS has a M_w range of 3000–4000 Da, which corresponds to ranges of m and n values: m = 30–38, n = 5–8.

Our group and others have previously investigated the properties of functionalized poly(dimethylsiloxane) (PDMS) materials before and after crosslinking [27]. In general, PDMS-based polymers are flexible, biocompatible, and relatively durable and stable in a variety of environments [28]. With longer building blocks, intrachain conformational reactions are hampered, making the polymer backbone more flexible [29]. PDMS is often modified before use through either bulk or surface modifications to improve mechanical strength or other properties [28]. Applications of functionalized PDMS polymers include protective coatings, wearable devices, medical systems, biomimetic materials, and robotics [30–32]. Bernkop-Schnürch and coworkers [33–35] have reported thiolated PDMSs for mucoadhesive applications due to its flexibility, thermal stability,

and biocompatibility [36]. Kulawik-Pióro et al. have demonstrated that thiolated PDMSs may be useful as skin protectants in topical creams [37]. Additionally, dual imine- and aryl disulfide-functionalized PDMS elastomers with good self-healability have been reported [13]. Partenhauser et al. [33] utilized amide coupling reactions between amine groups of (1-aminopropyl)methylsiloxane-dimethylsiloxane co-polymers and cysteine or mercaptopropionic acid to incorporate thiols into the thiolated silicone oils. In vitro mucoadhesion studies of thiolated and non-thiolated silicone oils showed enhanced mucosal adhesion for the thiolated compounds. Rheological measurements were performed after incubating thiolated silicone oils in I_2 solutions, and showed drastic increases up to 500-fold of the storage modulus [33]. Although excess I_2 was used to oxidize the thiolated silicone oils, no purification was mentioned. Several other articles have used similar methodologies to demonstrate rheological changes in the non-isolated disulfide-networks after oxidation [38–40].

Here, the disulfide networks are characterized after isolation to understand how changes to the reaction conditions can be used to tune the rheological properties of the resulting D-PDMS materials. We suspected, and confirmed, that the crosslinking conditions are very important in determining the properties of the oxidized materials. We hypothesized that altering the concentration of T-PDMS during its oxidation would result in products with different rheological properties, since polymer concentration has been demonstrated to regulate inter- and intra-chain crosslinking.

The conformation of a polymer in solution depends upon its concentration and the solvating ability of the solvent. In poor solvents, neutral flexible polymers adopt coiled conformations. As the solvating ability of the solvent increases, from 'poor' solvents to 'good' solvents [41] neutral polymers expand from coils and adopt random walk conformations, which have higher average end-to-end distances. If polymers aggregate, their chain conformations, can also be used to modulate the probability of intra- or inter-chain crosslink formation. In very dilute solutions, single-chain linear polymers can be crosslinked to produce single-chain polymer nanoparticles [42–44]. Interchain covalent crosslinks change the internal structure and thermomechanical properties of linear glassy polymers, and large proportions of interchain crosslinks can increase strength while decreasing toughness and processability [45].

This article describes how, for each of the two series of D-PDMS products, there is a T-PDMS concentration threshold above which products are solids, and below which products are liquids. To remove one variable, all crosslinking reactions have been conducted with a 25% group excess of oxidizing agent, I_2. Despite using excess oxidant, the D-PDMS materials ranged from solids to liquids, and exhibited enhanced thermal stability, relative to the corresponding T-PDMS starting polymers. Solution-state ^{1}H and ^{13}C nuclear magnetic resonance spectroscopy (NMR) and solid-state cross-polarization (CP/MAS) ^{13}C NMR spectroscopy were used to quantify the degrees of disulfide formation for the liquid and solid D-PDMSs, respectively. Those results indicate that all of the D-PDMS materials are >90% crosslinked. The rheological behaviors, including viscosities, of the liquid D-PDMSs are described. Additionally, the solid D-PDMSs exhibited unprecedented high degrees of swelling in hydrophobic solvents. Results from thermal studies, demonstrating that crosslinked PDMS materials are more stable thermally than their thiolated analogs are also described.

2. Materials and Methods

2.1. Materials

Acetone (Fisher, 99.9%), chloroform ($CHCl_3$, Sigma-Aldrich, Burlington, MA, USA $\geq$99%), chloroform-*d* ($CDCl_3$, Cambridge Isotope Laboratories Inc., Tewksbury, MA, USA, 99.8%), dichloromethane (DCM, Fisher, Waltham, MA, USA, >99%), diethyl ether (Et_2O, anhydrous, Fisher, 99.9%), ethanol (EtOH, The Warner Graham Company, Cockeysville, MD, USA, 200 proof), ethyl acetate (EtOAc, Fisher, 99.9%), hexanes (Fisher, 99.9%), hydrochloric acid (HCl, Fisher, certified ACS plus grade), iodine (I_2, Sigma Aldrich, $\geq$99.8%), magnesium

sulfate ($MgSO_4$, anhydrous, Sigma Aldrich, ≥99.5%), methanol (MeOH, anhydrous, Fisher, 99.9%), sodium thiosulfate ($Na_2S_2O_3$, anhydrous, J.T. Bakers Analyzed, Phillipsburg, NJ, USA, ≥99.8%), and triethylamine (Et_3N, Sigma Aldrich, ≥99%) were used as received. For liquid-liquid extractions, deionized water (DI water) was used, but for swelling studies, nanopure water (H_2O, ≤0.05 μS, Millipore, Burlington, MA, USA) was used.

SMS-042- [4–6% (3-mercaptopropyl) methylsiloxane]-dimethylsiloxane copolymer (4–6% T-PDMS, Gelest Inc., Morrisville, PA, USA, >97.5%) and SMS-142- [13–17% (3-mercaptopropyl) methylsiloxane]-dimethylsiloxane copolymer (13–17% T-PDMS, Gelest Inc., >97.5%) were heated twice from 21 °C to 49 °C at 0.5–0.15 mmHg over 1.5 h periods to remove a known impurity, octamethylcyclotetrasiloxane (D4), which was present at <5 wt% in the commercially received materials [46,47]. The flasks containing the T-PDMSs were weighed before and after each heating cycle; after two cycles, no change in mass was observed. The purities of 4–6% T-PDMS and 13–17% T-PDMS after treatment were estimated to be ≥97.5%. The treatment details and T-PDMS characterization are provided in the Supplementary Materials.

2.2. Methods

^1H, ^{13}C, and two-dimensional homonuclear ^1H-^1H correlation (COSY) NMR spectra of liquid samples were obtained on a 400 MHz Varian 400-MR spectrometer in $CDCl_3$ without a TMS reference at 25 °C. ^1H NMR spectra were collected with 128 scans and a 5 s relaxation time delay. Solution-state ^{13}C NMR spectra were collected with 10,000 scans and a 25 s relaxation time delay. Samples for solution-state ^{13}C NMR were prepared by dissolving ca. 50–100 mg of material in ca. 0.6 mL $CDCl_3$. The residual $CHCl_3$ peaks in the ^1H and ^{13}C spectra were set to 7.26 and 77.16 ppm, respectively, as reference peaks [48]. CP/MAS ^{13}C NMR spectroscopy of solid D-PDMS materials was performed on a Bruker Advance III 600 NMR spectrometer, operating at Larmor frequencies of 600.2 MHz (^1H), 150.9 MHz (^{13}C). A 5.0 mm triple resonance (^1H, ^{13}C, ^{15}N) E-free CPMAS Bio-solids probe was used. Solid D-PDMS materials were contained in Kel-F inserts within 4 mm ZrO2 rotors. CP/MAS ^{13}C NMR spectra of 13–17% D-$PDMS_{55wt\%}$, 4–6% D-$PDMS_{55wt\%}$, 13–17% D-$PDMS_{15wt\%}$, and 13–17% D-$PDMS_{6wt\%}$were obtained from 76.3, 58.9, 40.1, and 67.5 mg, respectively (see Table 1 for specific definitions). The temperature was held constant at 25.0 °C. Calibration was completed using KBr and adamantane [49]. For quantitative CP/MAS ^{13}C NMR measurements, the acquisition conditions were optimized following a procedure developed at NIST [50], and specifically involve the optimization of spin rate, contact time, and recycle delay. This resulted in the selection of spinning rate (4900 Hz), contact time (6000 μs), and recycle delay (5 s), along with a spectral width of 197.21 ppm, ramp. 100 for the ^1H-pulse shape during CP, tppm13 for the ^1H-pulse shape during LG-decoupling, and 8192–17152 scans. Data were acquired and analyzed using Topspin 3.2 (Bruker). NMR chemical shifts (δ) are reported in parts-per-million (ppm). All ^1H NMR spectra exhibited a peak at ca. 1.56 ppm (s), which can be attributed to water [48].

Table 1. Two series of disulfide-crosslinked (D-PDMS) materials formed during the oxidation of 4–6% T-PDMS and 13–17% T-PDMS at different solution concentrations; 1.25 molar eq. of I_2, with respect to the thiol groups, were included in all experiments.

D-PDMS Material	Thiol Monomer Substitution in T-PDMS	M_w Range (Da) of T-PDMS	Initial Concentration of T-PDMS [1]	Initial Concentration *in thiol* (M)	Product Phase
4–6% D-$PDMS_{2wt\%}$	4–6%	6000–8000	2 wt%	0.02	Liquid
4–6% D-$PDMS_{6wt\%}$	4–6%	6000–8000	6 wt%	0.06	Liquid
4–6% D-$PDMS_{15wt\%}$	4–6%	6000–8000	15 wt%	0.18	Liquid
4–6% D-$PDMS_{55wt\%}$	4–6%	6000–8000	55 wt%	0.47	Solid

Table 1. *Cont.*

D-PDMS Material	Thiol Monomer Substitution in T-PDMS	M_w Range (Da) of T-PDMS	Initial Concentration of T-PDMS [1]	Initial Concentration *in thiol* (M)	Product Phase
13–17% D-PDMS$_{1wt\%}$	13–17%	3000–4000	1 wt%	0.02	Liquid
13–17% D-PDMS$_{6wt\%}$	13–17%	3000–4000	6 wt%	0.16	Solid
13–17% D-PDMS$_{15wt\%}$	13–17%	3000–4000	15 wt%	0.32	Solid
13–17% D-PDMS$_{55wt\%}$	13–17%	3000–4000	55 wt%	1.14	Solid

[1] Because iodine was added to the thiol solutions dropwise, the concentrations decreased during the addition; see Table S1 for the solution concentrations after complete addition of the I_2 solutions.

Rheological measurements, including amplitude-sweeps (strain-sweep), frequency-sweeps, and flow curves were collected on an Anton Parr MCR 302 rheometer using stainless-steel parallel plates with a diameter of 25 mm (PP25). Measurements were recorded with a gap of 0.1 mm at 25 °C. Amplitude-sweeps were recorded from 0.01% to 100% strain at a fixed angular frequency of 1 rad/s. Frequency-sweeps were recorded from 0.1 to 100 Hz with strain fixed at 1% (i.e., within the linear viscoelastic region). Dynamic viscosity (η) was measured for shear rates between 0.1–100.0 s^{-1}.

Swelling behavior of solid products was evaluated in hexanes, ether, $CHCl_3$, EtOAc, DCM, acetone, EtOH, MeOH, and ultrapure water using a procedure adapted from Yu et. al. [27]. A small screw-cap vial was filled with 50.0 ± 2.5 mg of cross-linked polymer and 3 mL of solvent was added. After the addition of solvent, vials were capped tightly for 24 h. Then, the swollen polymer pieces were rapidly blotted on filter paper to remove excess solvent and immediately weighed.

Paired thermogravimetric analysis (TGA) and mass spectrometry (MS) measurements were conducted with a TA Instruments model Q5000 thermogravimetric analyzer and a Balzers Prisma EI FER vacuum mass spectrometer. The furnace of the thermal gravimetric analyzer was connected to the mass spectrometer and vacuum with a capillary tube. Experiments were conducted as follows: approximately 10 mg samples were placed in a platinum TGA pan. Nitrogen was flushed through the furnace (10 mL/min) for 30 min to purge the system before conducting experiments. The mass spectrometer was configured to scan a particular mass-to-charge ratio range and to subtract the background ion current from each scan. A background scan was collected after the 30 min nitrogen purge period, after which TGA was begun. TGA was conducted using the following protocol: the sample was equilibrated at 30 °C for 10 min, and then heated from 30 °C to 350 °C at a rate of 5 °C/min. MS measurements and TGA were started at the same time; however, there was a lag between the formation of TGA decomposition products and their detection by MS. The lag time was determined (as described in the Supplementary Materials), and all results were corrected to account for the detector lag time. When not paired with mass-spectrometry, TGA was conducted on a TA Instruments model Q50 instrument. Approximately 10 mg of material was placed in a platinum pan, which was equilibrated at 30 °C for 5 min and then heated from 30 °C to 600 °C at a rate of 10 °C/min.

3. Results and Discussion

3.1. Starting Materials

Two types of T-PDMS (Figure 1) with 4–6% and 13–17% thiolated comonomers (mass average molar weight (M_w): 6000–8000 Da and 3000–4000 Da, respectively) were oxidized with 1.25 molar eq. of I_2, with respect to the thiol groups to produce disulfide-crosslinked D-PDMS materials. The thiol substitution percentages, calculated from ^{1}H NMR peak areas, indicated that 4–6% T-PDMS and 13–17% T-PDMS contained 4 mol% and 19 mol% of thiol groups, respectively.

3.2. Synthesis of D-PDMS Materials

The oxidation of a generic thiol (RSH) to a disulfide (RSSR) by I_2 is shown in Equation (1). The corresponding reduction in a disulfide to thiols involves the addition of electrons rather

than their removal. Details of the actual processes can be found in many sources, including references [19] and [23].

$$I_2 + 2RSH \rightleftharpoons RSSR + 2HI \quad (1)$$

The equilibrium in Equation (1) lies far to the right [19]. An advantage of using I_2 as the oxidant is that it does not oxidize thiols beyond the disulfide form under the conditions employed [23].

Both 4–6% T-PDMS and 13–17% T-PDMS were oxidized with I_2 to form D-PDMS materials; details are included in the Supplementary Materials. A range of solid and liquid D-PDMSs were formed (Table 1). The product names in the last column of Table 1 are in the format: x-y% D-PDMS$_{\#wt\%}$. "x-y%" designates the mol% of thiolated monomers in the T-PDMS reactant (either 4–6% or 13–17%), "D" indicates that the material is a crosslinked disulfide, formed from oxidation of the corresponding T-PDMS. The "#wt%" subscript indicates the initial T-PDMS concentration used during the oxidation reaction.

A total of 4–6% T-PDMS and 13–17% T-PDMS were oxidized in solution at four (initial) solution concentrations: 1- 2wt%, 6wt%, 15wt%, and 55wt%. Details are included in the Supplementary Materials. Because the exact mass average molar weights of the T-PDMSs were unknown, the molar concentrations of thiol reported in Table 1 were calculated using the method described in the Supplementary Materials. Prior to each synthesis, the solutions were sparged with N_2. All reactions were conducted at room temperature using 1.25 molar eq. of I_2 in $CHCl_3$, which was slowly added dropwise to stirred solutions of a T-PDMS (1 molar eq.) and Et_3N (1 molar eq.) in $CHCl_3$. Table 1 expresses the initial concentration of T-PDMS prior to the addition of the I_2 solution, and Table S1 reports the final concentration of T-PDMS after the addition of the I_2 solution. Visual observations indicate that the initial polymer concentration is the more important factor: for most syntheses yielding solid products, a gel-like phase was observed after the first few drops of I_2 solution were added. Regardless, the initial polymer conformation is one of the most important variables governing the extent of inter- and intra-chain crosslinks [51]. When the first disulfide crosslinks form, either within or between chains, network formation permanently locks local conformations about the nascent disulfide bonds. Consequently, the free thiol oxidation rate should be decreased.

To promote intrachain crosslinking over interchain crosslinking [52], T-PDMSs were first crosslinked under initially relatively dilute conditions, resulting in oil/liquid products (e.g., 4–6% D-PDMS$_{2wt\%}$ and 13–17% D-PDMS$_{1wt\%}$). The synthesis of 4–6% D-PDMS$_{2wt\%}$ was followed by ^{1}H NMR spectroscopy to optimize the reaction time. Because spectra did not change over periods of two or three days, the syntheses of other liquid D-PDMSs were conducted for three days. The ^{1}H NMR spectra of the liquid D-PDMSs exhibit features consistent with nearly complete oxidation of the thiol groups to disulfide groups (Figure 2).

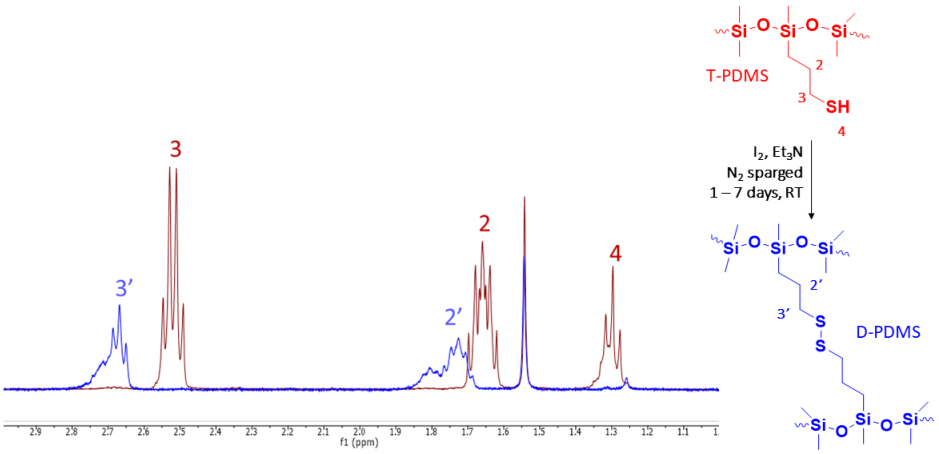

Figure 2. ^{1}H NMR spectra of 4–6% T-PDMS (red) and 4–6% D-PDMS$_{2wt\%}$ (blue).

Solution concentrations were then increased in subsequent reactions, to promote more interchain crosslinking. When the initial concentration of T-PDMS in the reaction solution was ≥55wt% (for 4–6% T-PDMS) or ≥6wt% (for 13–17% T-PDMS), solid products were formed. The solid products listed in Table 1 could not be solubilized in any of the tested solvents (which included hexanes, ether, $CHCl_3$, EtOAc, DCM, acetone, EtOH, MeOH, water, and HCl (aq)). Those reactions were allowed to proceed for 7 days. The formation of a solid was obvious during these syntheses, except in the synthesis of 13–17% D-$PDMS_{6wt\%}$. Solid D-PDMSs were isolated from the reaction mixtures after swelling in solvents and decanting the solution phase through a filter, as described in the Supplementary Materials. The 13–17% D-$PDMS_{6wt\%}$ product was an anomaly, however. Initially, 13–17% D-$PDMS_{6wt\%}$ was an oil, and miscible with $CHCl_3$, so a solution of 13–17% D-$PDMS_{6wt\%}$ (in $CHCl_3$) was treated with a series of aqueous washes to remove unreacted I_2, as described in the Supplementary Materials. After the final wash step, but prior to solvent removal, 13–17% D-$PDMS_{6wt\%}$ was gelled by $CHCl_3$. After removing the $CHCl_3$, 13–17% D-$PDMS_{6wt\%}$ was a solid that remained insoluble in all tested solvents, including $CHCl_3$.

A concentration of T-PDMS above which solid products form, and below which liquids or oils form, can be described. That concentration is not the same for 4–6% T-PDMS and 13–17% T-PDMS. Of the D-$PDMS_{1wt\%}$, only 13–17% formed a liquid from the oxidation of 13–17% T-PDMS at the lowest tested concentration. Conversely, only 4–6% D-$PDMS_{55wt\%}$, formed during the oxidation of 4–6% T-PDMS at the highest tested concentration, was a solid. Although both 4–6% T-PDMS and 13–17% T-PDMS show concentration-dependent product phases, it is unsurprising that they have different concentration boundaries. For a reaction conducted with a given weight percentage of T-PDMS in solution, the 13–17% T-PDMS reaction solution was more viscous than that of 4–6% T-PDMS; the viscosity of neat 13–17% T-PDMS is higher (see Section 3.5).

Solvent-free oxidation of 13–17% T-PDMS was attempted, by mixing I_2, and Et_3N with the neat polymer. However, comparison of the ^{1}H NMR spectra before and after the reaction indicated that the polymer backbone had fractured, since the integration of the methylsiloxane peak decreased substantially, from 40.7H to 23.6H, relative to the starting material (Figure S15), and several new impurity peaks emerged (described in the Supplementary Materials). Although the vial was mechanically rotated to mix the reagents during the reaction, it is possible that the Et_3N was poorly distributed in the viscous mixture, and may have inhibited neutralization of HI (formed in situ).

3.3. Characterization of Residual Thiol Content in Liquid Products

The ^{1}H NMR spectra in Figure 2 are labelled with key diagnostic peaks that distinguish T-PDMS and liquid D-PDMS products, including the disappearance of the -CH_2S**H** peak (peak 4) and the downfield shift of the α peak (peaks 2 and 2′).

The ^{1}H NMR spectra of the liquid D-PDMS materials (Figures S10–S11 and S13–S14) include a small peak of unknown origin at 1.26 ppm, which overlaps the -CH_2S**H** peak region. The COSY NMR spectrum of 4–6% D-$PDMS_{2wt\%}$ (Figure S18) indicates that the peak at 1.26 ppm is not correlated to the α, β, or γ methylene protons adjacent to the disulfide.

All of the ^{1}H NMR spectra of the liquid D-PDMSs exhibit a small peak at 0.74 ppm (m), possibly due to changes in the chemical environment of the γ-methylene protons after oxidation. Although the -CH_2S**H** peak could not be used to quantify residual thiol in the liquid D-PDMS materials, the -C**H_2**SH and -C**H_2**SS- peak of the thiol and disulfide, respectively, do not overlap, providing a useful diagnostic for this determination. As shown in Figure 3 for 4–6% T-PDMS and its oxidation product, 4–6% D-$PDMS_{6wt\%}$, the chemical shift of -C**H_2**SH peak is downfield, relative to the -C**H_2**SS- peak.

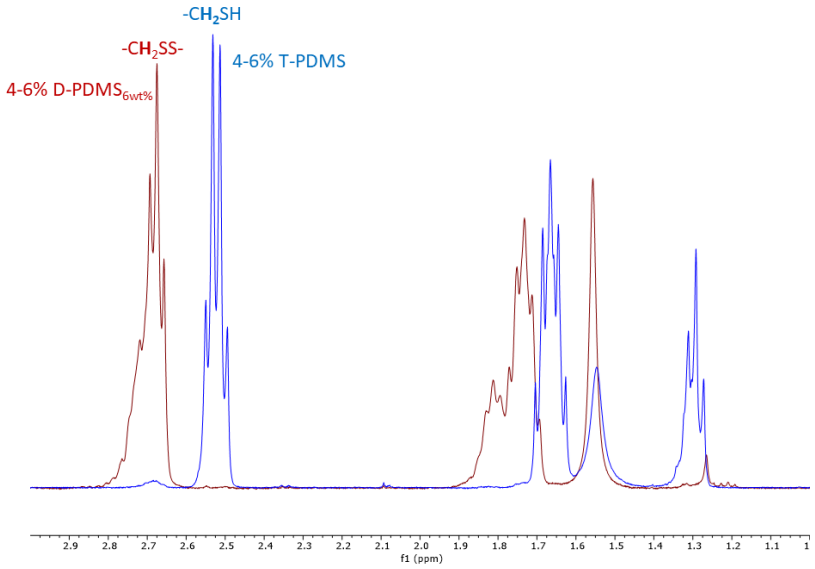

Figure 3. ^{1}H NMR spectra of 4–6% T-PDMS (blue) superimposed upon its oxidation product 4–6% D-PDMS$_{6wt\%}$ (red). The α methylene protons of the thiol (-C**H$_2$**SH) and the disulfide (-C**H$_2$**-SS-) are indicated.

The integration values in the region associated with the -C**H$_2$**SH and -C**H$_2$**SS- peak were used to calculate the percent of residual thiol remaining in the liquid D-PDMSs (Table 2). Based on Table 2, all liquid D-PDMS materials are extensively crosslinked; at most, only 5% of the initial thiols remain in the liquid D-PDMS materials after oxidation. Despite nearly complete thiol oxidation in these networks, these liquids all exhibit flow, which indicates that a relatively large proportion of the crosslinks must be intrachain.

Table 2. Proton integrations of the -C**H$_2$**SH peaks of liquid D-PDMSs and estimates of percentages of residual thiol.

Oxidation Product	Integration Value of the Protons α to the Thiol Group [1]	Calculated Percentage of Thiol Remaining after Oxidation
4–6% D-PDMS$_{2wt\%}$	0.01	0.5%
4–6% D-PDMS$_{6wt\%}$	0.00	0%
4–6% D-PDMS$_{15wt\%}$	0.02	1%
13–17% D-PDMS$_{1wt\%}$	0.07	3.5%

[1] Integrations normalized so that the total areas of the -C**H$_2$**SH and -C**H$_2$**SS- peaks is 2H.

3.4. Characterization of Residual Thiol Content in Solid Products

Due to their insolubility in all tested solvents, the solid D-PDMSs were challenging to characterize, but solid-state CP/MAS ^{13}C NMR was the analytical tool employed. Solution-phase ^{13}C NMR spectra of 4–6% T-PDMS and its liquid product, 4–6% D-PDMS$_{2wt\%}$ were compared, and peaks associated with the thiol and disulfide forms were assigned (Figure S16). After oxidation of 4–6% T-PDMS to 4–6% D-PDMS$_{2wt\%}$, the -**C**H$_2$SH groups were converted to -**C**H$_2$SS- groups, resulting in a downfield shift (from 28 ppm to 42.4 ppm).

Although the solution-phase ^{13}C NMR spectra of 4–6% T-PDMS and 4–6% D-PDMS$_{2wt\%}$ include some minor peaks of unknown origin (described in the Supplementary Materials), the solution-state ^{13}C NMR of 4–6% D-PDMS$_{2wt\%}$ (Figure S12) and the solid-state CP/MAS ^{13}C NMR spectra of the solid DPDMSs (Figure 4) include the same peaks; those associated with the disulfide are at 42.4 and 23.1 ppm. If thiol groups are present, the quantity must be below our limit of detection for ^{13}C NMR detection. Considering the experimental conditions and amounts of materials used for collecting the CP/MAS ^{13}C NMR

spectra [53,54], about 2 μmol of material, corresponding to less than 0.1% of thiol. should have been detectable.

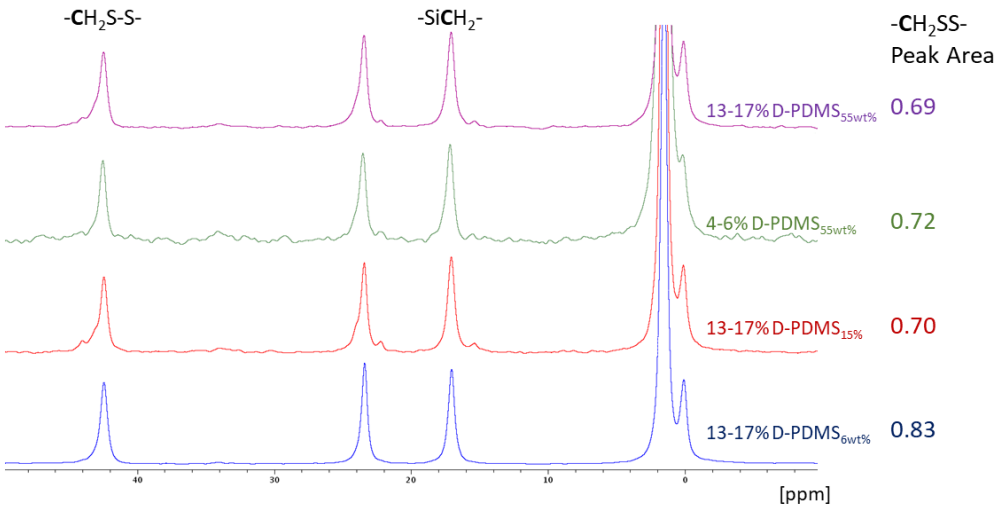

Figure 4. Solid state CP/MAS ^{13}C NMR spectra of solid D-PDMS materials with -**C**H_2SS- peak areas. The areas of the -**C**H_2SS- peaks (42.4 ppm) were normalized with respect to the -Si**C**H_2- peaks (17.1 ppm), which were set to 1C in each spectrum.

Although the ^{13}C NMR spectra of the four solid D-PDMS materials include the same peaks, the α methylene carbon peak (-**C**H_2SS-) areas are different when normalized with respect to the γ methylene carbon (-Si**C**H_2-) peak (17.1 ppm). The areas of the -**C**H_2SS- peaks (Figure 4) indicate the relative amounts of disulfide groups in these materials.

Three of the solids were synthesized from 13–17% T-PDMS, and one was synthesized from 4–6% T-PDMS. The peak area integrations with respect to the 17.1 ppm peaks range from 0.69 to 0.83. The uncertainty is estimated to be ca. 0.03 based on signal-to-noise ratios and peak shapes. Because the ratio of 13–17% D-PDMS$_{6wt\%}$ is significantly higher than the average of the other solids (0.70 ± 0.02), it appears to be significantly more crosslinked. A total of 13–17% D-PDMS$_{6wt\%}$ was mentioned previously because it solidified during purification. It also swells the least of all solid D-PDMS materials, consistent with a significantly more crosslinked product.

3.5. Physical Properties of Liquid Crosslinked Materials

Frequency sweeps from rheological measurements are shown in Figure 5 for the T-PDMSs and liquid D-PDMS materials. Frequency sweeps were performed with 1% strain, which is in the linear viscoelastic region (LVR), based on amplitude-sweep measurements (Figures S19 and S20). All frequency sweeps had crossover points at relatively high angular frequencies (above 300 rad·s^{-1}), above which the storage modulus (G′) became higher than the loss modulus (G″). After 13–17% T-PDMS was crosslinked to 13–17% D-PDMS$_{1wt\%}$, the crossover point was at a higher angular frequency, and the crossover modulus was higher (Figure 5a). Overall, crosslinking dilute concentrations of 13–17% T-PDMS led to a decrease in G′ and an increase in G″, relative to 13–17% T-PDMS. Although the viscosity of 4–6% T-PDMS was too low to obtain a frequency sweep using our rheometer, frequency sweeps of the liquid 4–6% D-PDMS materials were measurable (Figure 5b). Both 4–6% D-PDMS$_{2wt\%}$ and 4–6% D-PDMS$_{6wt\%}$ exhibited a trend like that of the 13–17% T-PDMS and 13–17% D-PDMS$_{1wt\%}$, respectively, although the changes were less pronounced. G′ and G″ increased for 4–6% D-PDMS$_{15wt\%}$, relative to the other liquid 4–6% D-PDMS materials, but a crossover point was not reached at frequencies up to 600 rad·s^{-1}; however, the data suggest that G′ and G″ might reach the crossover point slightly above this frequency (Figure 5b).

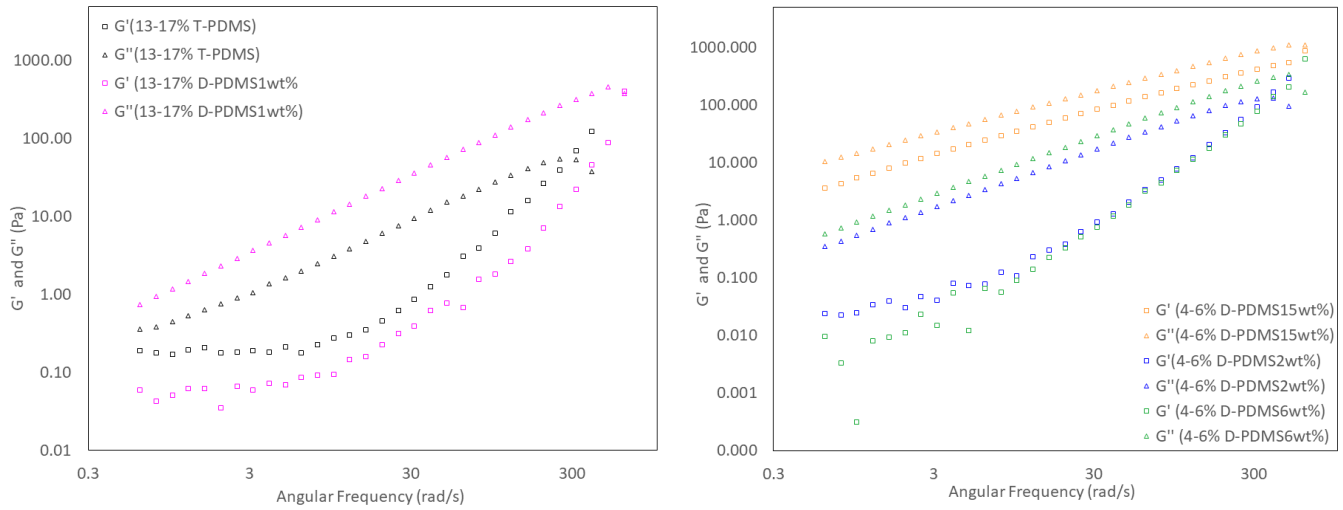

(**a**) (**b**)

Figure 5. Frequency sweeps at 1% strain: (**a**) 13–17% T-PDMS and liquid 13–17% D-PDMS$_{1wt\%}$; (**b**) liquid 4–6% D-PDMS materials.

Flow curves, plotting viscosity versus shear rate, are shown in Figure 6 for the T-PDMS materials and their liquid D-PDMS oxidation products. The viscosities of the materials are nearly constant as a function of shear rate, except for 4–6% D-PDMS$_{15wt\%}$, which exhibits lower viscosities at higher shear rates. An amount of 13–17% T-PDMS had a lower viscosity than its only liquid oxidation product, 13–17% D-PDMS$_{1wt\%}$ (Figure 6a); similarly, 4–6% T-PDMS had a lower viscosity than each of its liquid oxidation products (Figure 6b). Therefore, under the crosslinking conditions employed, the viscosities of all liquid D-PDMS materials increased upon crosslinking, indicating that both inter- and intra-chain crosslinks were formed. If intrachain crosslinks had formed exclusively in any of the D-PDMS, the viscosity would have been lower than that of the parent T-PDMS, because intrachain crosslinks render the structures more compact [51]. Additionally, higher concentrations of 4–6% T-PDMS during crosslinking resulted in liquid 4–6% D-PDMS materials with higher viscosities. An amount of 4–6% D-PDMS$_{15wt\%}$ had the highest viscosity of the liquid 4–6% D-PDMS materials at all measured shear rates.

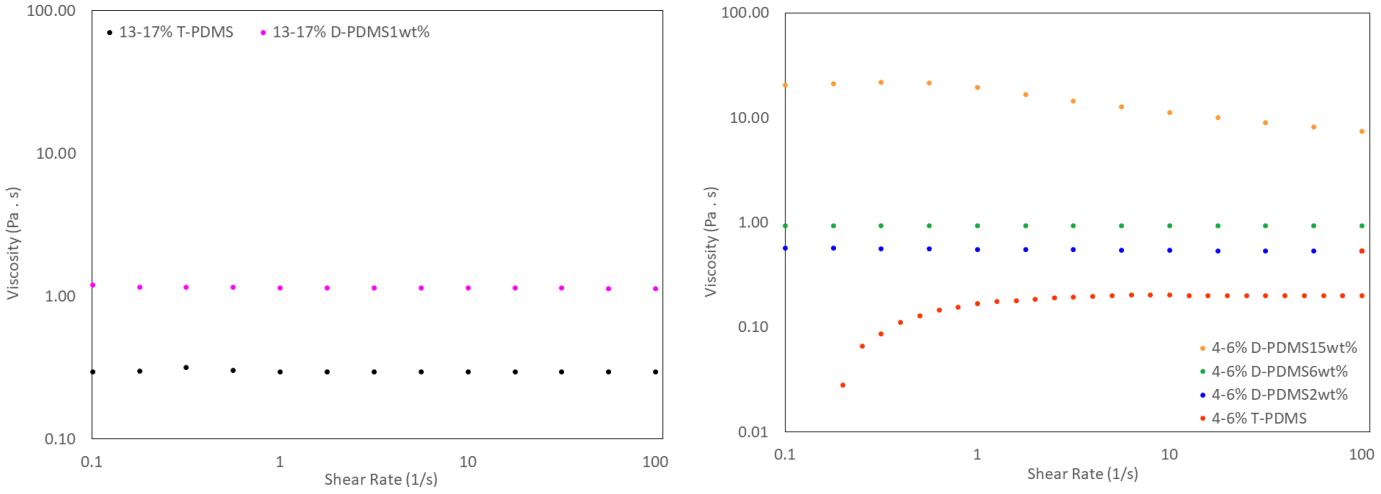

(**a**) (**b**)

Figure 6. Flow curves of (**a**) 13–17% T-PDMS and its liquid product, 13–17% D-PDMS$_{1wt\%}$ (**b**) 4–6% T-PDMS and its liquid 4–6% D-PDMS products.

Kuhn and Balmer [51] developed a model to relate crosslinked product viscosity to the degree of inter- and intra-chain crosslinking for poly(vinyl alcohol)s. According to their model, the polymer concentration above which interchain crosslinking becomes dominant can be determined by plotting the polymer crosslinking concentration against the viscosity of the neat crosslinked product. The inflection point of the curve indicates the crosslinking concentration at which interchain crosslinking becomes dominant. The initial concentration of 4–6% T-PDMS during crosslinking has been plotted against the zero-shear viscosity (η_0) of the corresponding 4–6% D-PDMS product in Figure 7. Although this plot provides only a very rough estimate of the critical concentration at which interchain crosslinking becomes dominant, because of the limited number of concentrations explored it is sufficient to see that the region of large change fits within our other data.

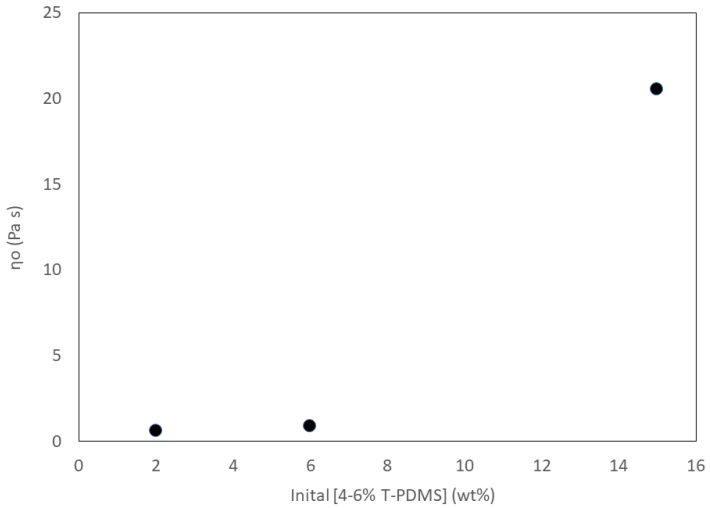

Figure 7. Plot of the zero-shear viscosities (η_0) of liquid 4–6% D-PDMSs versus initial 4–6% T-PDMS concentrations.

As the concentration of 4–6% T-PDMS increases from 5 to 15 wt%, the viscosity of the product increased sharply, indicating that interchain crosslinking becomes dominant above 5–15wt%. Although intrachain crosslinking is more important when the oxidations are conducted at T-PDMS concentrations $\leq$ 5 wt%, it does not occur exclusively: 4–6% D-PDMS$_{2wt\%}$ and 4–6% D-PDMS$_{6wt\%}$ exhibit higher viscosities than 4–6% T-PDMS (η_o of 4–6% T-PDMS = 0.003 Pa·s). If intrachain crosslinks had formed exclusively, the crosslinked products, 4–6% D-PDMS$_{2wt\%}$ and 4–6% D-PDMS$_{6wt\%,}$ would have been less viscous than the 4–6% T-PDMS [51].

3.6. Swelling Studies of Solid Crosslinked Materials

For materials that do not dissolve in most solvents, swelling can be used to describe the nature of the polymer-solvent interactions [55]. The swelling behavior of the solid D-PDMS materials was assessed after the samples were placed in capped vials with a large excess of solvent at room temperature for 24 h. The percent swelling by mass (S%) was calculated using Equation (2), where m_i and m_f are the initial and final (swollen) masses, respectively:

$$\frac{m_f - m_i}{m_i} \times 100\% = S\%, \quad (2)$$

The percent swelling by volume (V%) was calculated using the densities of each liquid and the density of the original T-PDMS materials (ca. 0.98 g/mL). The final and initial volumes were used in place of the final and initial masses in equation 2, respectively, to obtain V%. The swelling data in Figure 8 is expressed by V%. For comparison, a plot of D-PDMS swelling by mass percent (S%) is shown in Figure S21.

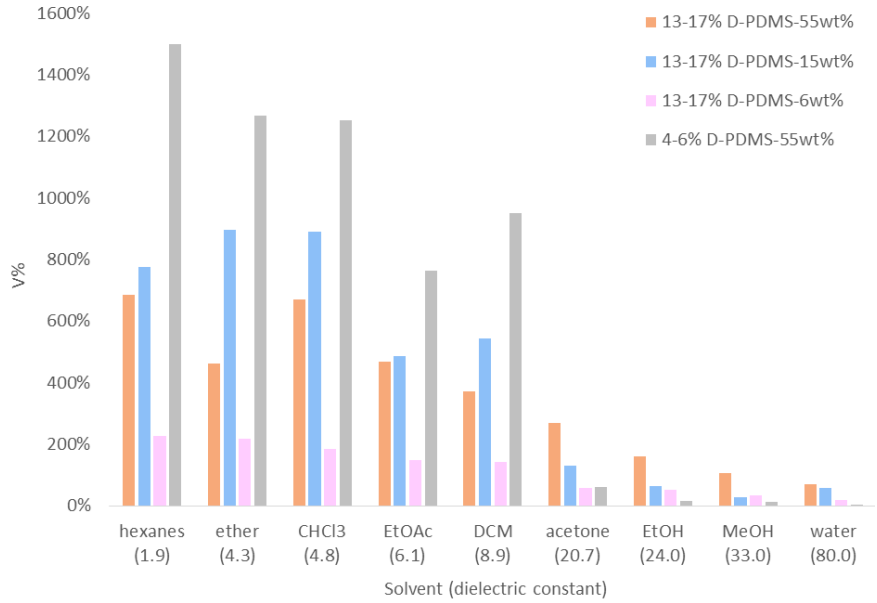

Figure 8. Percent increases of D-PDMS volume (V%) in various solvents. Note: the dielectric constants (ε) of the solvents increase from left to right; values are provided in parentheses under each solvent name.

Swelling volumes and masses are expected to be lower for more highly cross-linked networks, and swelling should be enhanced when the solvent and network have similar polarities. In solvents of low to moderate polarity, the solid 4–6% D-PDMS$_{55wt\%}$ swelled to a much greater extent than the solid 13–17% D-PDMSs. This trend was expected: on a per crosslink basis that is normalized for sample mass, 4–6% T-PDMS has fewer thiol groups, and, thus, fewer crosslinking sites per gram than does 13–17% T-PDMS.

Colby plotted polymer concentration versus M_w for flexible neutral polymers in a good solvent, and indicated three concentration regimes [41]. One is in the dilute concentration regime for polymers of low mass average molar weight. Considering the T-PDMS M_w values, and comparing them with the data compiled by Colby, solutions of T-PDMS at 1–2 wt% would fall in the dilute regime. The M_w values of the T-PDMS materials (Figure 1) are significantly below the critical entanglement range of PDMS, 24,500 Da [56]. The two other concentration regimes can be defined based on the critical overlap concentration (c*) and the entanglement concentration (c_e), both of which are directly proportional to M_w. The c* is defined as the point where the concentration of excluded polymer volume (due to overlap) is equal to the concentration of the polymer in solution. At c_e, there is an abrupt increase in the power law exponent describing the relationship between polymer concentration and solution viscosity (for polymers dissolved in good solvents), as chains become entangled [41]. When the polymer concentration is >c* but <c_e, polymers are partially entangled, and the degree of entanglement increases as the concentration increases toward the c_e. Considering the T-PDMS M_w values, and comparing them with the data compiled by Colby, solutions of T-PDMS at 55 wt% would fall in the regime defined by concentrations between c* and c, (i.e., polymer chains are tightly packed, but not fully entangled).

Consistent with the hypothesis that the solid 13–17% D-PDMS materials synthesized from more concentrated solutions are more entangled than those formed from lower concentrations of 13–17% T-PDMS, the 13–17% D-PDMS$_{15wt\%}$ swelled slightly more than 13–17% D-PDMS$_{55wt\%}$. A higher concentration of T-PDMS during the oxidation reaction should favor crosslinks between more heavily entangled chains, with each chain having a shorter average end-to-end distance. At higher concentrations, the average distance between two chains will also decrease, resulting in a higher proportion of interchain crosslinks, relative to intrachain crosslinks.

Because 13–17% D-PDMS$_{6wt\%}$ was synthesized from the 13–17% T-PDMS solution with the smallest degree of entanglement, the 13–17% D-PDMS$_{6wt\%}$ was expected to swell solvents to the greatest extent of the solid 13–17% D-PDMS materials. However, 13–17% D-PDMS$_{6wt\%}$ had significantly lower V% values than the other solid 13–17% D-PDMSs. CP/MAS ^{13}C NMR spectra indicate that the solid D-PDMS materials are similar. However, the observation that the -**C**H$_2$S-S**C**H$_2$- peak area in the 13–17% D-PDMS$_{6wt\%}$ spectrum is ca. 20% higher (ca. 0.8) than the other solid D-PDMSs (ca. 0.7) indicates more disulfide crosslinking; the 13–17% D-PDMS$_{6wt\%}$ has a higher crosslink density than the other solids, and it is this structural feature that appears to decrease its ability to be swelled. The 13–17% D-PDMS$_{6wt\%}$ is also significantly less sticky, and more brittle than the other solid D-PDMS materials, which is consistent with a higher degree of interchain crosslinking.

Table 3 provides the Hildebrand solubility parameters (δ) and dielectric constants (ε) for each of the solvents examined. An amount of 4–6% D-PDMS$_{55wt\%}$ exhibited the highest V% values overall. Although our preferred metric is percent volume increase (V%) because it accounts for differences in solvent densities, swelling by mass percent increase (S%) is more commonly reported in the literature. Table 3 reports the swelling results for 4–6% D-PDMS$_{55wt\%}$ based on volume (V%), along with corresponding calculated V% values from S% for crosslinked PDMSs [27,57,58]. The V% values were calculated by multiplying the reported S% values by the ratio of the polymer and solvent densities, and the density of the polymer was assumed to be 0.98 g/mL Table S3 provides the S% values from the literature and for 4–6% D-PDMS$_{55wt\%}$. Lee et al. ranked the ability of the solvents in Table 3, among others, to swell hexagonally shaped pieces of crosslinked PDMS; the ratio of the swollen and non-swollen length across the hexagon was used to define a swelling ratio [55]. In lieu of a direct comparison between these ratios and the S% or V% values, the relative solvent swelling rankings reported by Lee et al. are provided in Tables 3 and S3, respectively. Overall, the solvent rankings for 4–6% D-PDMS$_{55wt\%}$ are similar to those reported by Lee, especially when both V% and S% rankings are considered. In both cases, a strong preference for solvents with lower ε values was observed; swelling ability was poorly correlated with δ [55]. For the solid D-PDMS materials, a better correlation exists between the V% and dielectric constant of a solvent.

Table 3. Solvent Hildebrand solubility parameter (δ), dielectric constant (ε), and swelling ranking *based on volume* (where 1 is best) for 4–6% D-PDMS$_{55wt\%}$ and other crosslinked poly(dimethylsiloxane) (PDMS) materials.

Solvent	δ [55]	ε [59,60]	Relative Swelling Rank from Ref. [55] [1]	4–6% D-PDMS$_{55wt\%}$		PDMS-Based Materials in the Literature (V%)		
				Swelling Rank (Based on V%)	V%	Ref. [27] [2]	Ref. [57] [1]	Ref. [58] [3]
hexanes	7.3	1.9 [4]	3	1	1500%	580%	190%	
ether	7.5	4.3	2	2	1270%	500%	200%	
$CHCl_3$	9.2	4.8	1	3	1250%	700%		
EtOAc	9.0	6.1	5	5	760%	540%		80%
DCM	9.9	8.9	4	4	950%	520%	140%	
acetone	9.9	20.7	6	6	60%	120%		40%
EtOH	12.7	24.0	7	7	20%	30%	10%	10%
MeOH	14.5	33.0	8	8	10%			
water	23.5	80.0	9	9	>10%	0%	0%	

[1] References [55,57] data for Sylgard 184 silicone, a two-part PDMS elastomer prepared with 10:1 (wt:wt) ratio of PDMS base; [2] Reference [27] data for 3-aminopropylmethylsiloxane-dimethylsiloxane copolymer with 6–7% amino content, after crosslinking with CS_2; [3] Reference [58] data for dense silicone rubber samples prepared from a two-part system comprised of 10: 1 (wt:wt) vinyl terminated silicone oil: silane tetrafunctional compounds; [4] ε of n-hexane.

In Table 3, swelling data (V%) are shown for three crosslinked PDMS materials reported in the literature. For solvents with lower dielectric constants than acetone, 4–6%

D-PDMS$_{55wt\%}$ exhibited significantly higher V% values than in the literature. The swelling of hexanes by 4–6% D-PDMS$_{55wt\%}$ is nearly three times greater than the previously highest reported value. Possible applications for such a material could include oil spill remediation [27,61].

3.7. TGA and TGA/MS Studies

The thermal decompositions of T-PDMS and D-PDMS materials were measured using TGA (Figures S22–S29). Thermal decomposition onset temperatures of the D-PDMS materials ranged between 295 and 310 °C, which is consistent with data reported for other dialkyl disulfides [21]. The thermal decomposition onset temperatures of the T-PDMSs were much lower, between 60 and 85 °C. After the onset point, T-PDMS thermograms exhibited smooth, steady weight loss that slowly led to PDMS backbone decomposition. This was surprising, because aliphatic thiols are expected to decompose ca. 200 °C above the analogous disulfide, which, itself, should decompose above 250 °C. Thermal decomposition is more difficult to achieve for thiols because the RS—H and R—SH homolytic bond dissociation energies are about 100 kJ/mol higher than for the R—SS—R and R—S—S—R groups of disulfides [62,63]. Although it is surprising that the thiol forms decomposed at a lower temperature than the disulfides, crosslinking can sometimes result in increased thermal stability [64]. Paired TGA-MS was used to understand the thermal decomposition of the T-PDMS and D-PDMS materials. Decomposition of aliphatic thiols and disulfides produces H_2S (34.09 amu), sulfur, and smaller alkyl sulfides [65]. The paired TGA-MS experiments detected ions with the mass of H_2S after the onset of weight loss (between 295 and 310 °C) in the corresponding D-PDMS thermograms, indicating that the onset of thermal decomposition is associated with the decomposition of disulfide crosslinks (Figure S9). Conversely, close to the onset of thermal decomposition of 13–17% T-PDMS (82 °C), ions associated with the thermal decomposition of sulfur groups were not detected by MS (Figures S30 and S31). However, H_2S and S-related ions were detected at a much higher temperature (ca. 309 °C) during the 13–17% D-PDMS decomposition, indicating that without crosslinking, T-PDMS begins to decompose (or lose mass) for reasons unrelated to the decomposition of thiol pendant groups. It is also possible that RS$^{\cdot}$ pairs in the D-PDMS materials are held in positions favoring S-S bond reformation during heating, which may favor radical (re)coupling and (re)formation of disulfide bonds. However, further experimentation will be required to determine the importance of each of these possibilities. By crosslinking T-PDMS to liquid or solid D-PDMS materials, the thermal stability of the functionalized PDMS was increased, even though disulfides should be more thermally labile than thiols.

4. Conclusions

A range of disulfide-crosslinked liquid and solid D-PDMS materials was produced by oxidizing the thiol groups of two series of T-PDMS at various concentrations. We note that this procedure can be adapted easily to crosslink a wide range of thiolated polymers. Characterization data suggest that the liquid D-PDMS materials are chemically similar, despite having different viscosities. This observation indicates that inter- and intra-chain crosslinking was regulated by the T-PDMS concentrations during oxidation. Similarly, the solid-state ^{13}C NMR data suggest that the degree of crosslinking in the solid D-PDMS materials is similar (with the exception of 13–17% D-PDMS$_{6wt\%}$). However, their swelling behaviors differ, possibly due to the degree of chain entanglements in each of the networks. Perhaps of greatest interest is the demonstration that a range of materials with different viscoelastic properties was formed simply by tuning the ratio of thiolated and non-thiolated co-monomers in the T-PDMS and/or the T-PDMS concentration during oxidation. The thermal stabilities of both solid and liquid materials increased after the formation of disulfide-crosslinks. The viscosities of some of the liquid D-PDMSs are less than one order of magnitude larger than their parent T-PDMSs, yet are much more stable thermally.

TGA-MS data were used to determine that the onset of D-PDMS thermal decomposition is associated with reaction of the sulfur containing pendant groups.

In the future, it would be interesting to explore these reactions using different equivalents of iodine, because they might result in the formation of solid D-PDMS products that are more (or less!!) processable than the ones produced here. Based on the swelling data, studies considering the selective removal of oil from contaminated aquifers [27,61] may be possible. Because each solid D-PDMS has a lower density than water, and little ability to be swelled by water, they would be expected to float if swollen by low density (<1 g/mL) organic contaminants. An important future experimental direction would be to determine the conditions under which a D-PDMS can be reduced to the corresponding T-PDMS (and then re-oxidized) to the D-PDMS, and the extents to which the regenerated T-PDMS and D-PDMS recover their initial material properties.

Supplementary Materials: The following supporting information can be downloaded at: https://www.mdpi.com/article/10.3390/macromol3010004/s1, Figure S1: ^{1}H NMR spectrum of as-received 4–6% T-PDMS; Figure S2: ^{1}H NMR spectrum of purified 4–6% T-PDMS; Figure S3: Structure of 4–6%T-PDMS; Figure S4: ^{13}C NMR spectrum of purified 4–6% T-PDMS; Figure S5: ^{1}H NMR spectrum of purified 13–17% T-PDMS; Figure S6: ^{13}C NMR spectrum of purified 13–17% T-PDMS; Figure S7: TGA thermogram showing water lost from a wet molecular sieve as a function of time the paired TGA-MS experiment; Figure S8: Mass spectrum of 13–17% T-PDMS$_{55wt\%}$ from the paired TGA-MS experiment; Figure S9: TGA thermogram of 13–17% D-PDMS$_{55wt\%}$ correlating MS ion detection start and end times with the TGA thermogram times, temperatures, and mass percentages. TGA thermogram of 13–17% D-PDMS$_{55wt\%}$, correlating the ion detection start and end time with the times, temperatures, and percentages of remaining mass in the TGA thermogram; Figure S10: ^{1}H NMR spectrum of 4–6% D-PDMS$_{6wt\%}$; Figure S11: ^{1}H NMR spectrum of 4–6% D-PDMS$_{2wt\%}$; Figure S12: ^{13}C NMR spectrum of 4–6% D-PDMS$_{2wt\%}$; Figure S13: ^{1}H NMR spectrum of 4–6% D-PDMS$_{15wt\%}$; Figure S14: ^{1}H NMR spectrum of 13–17% D-PDMS$_{1wt\%}$; Figure S15: ^{1}H NMR spectra of 13–17% T-PDMS and the oxidation product formed under solvent-free conditions; Figure S16: Solution-Phase ^{13}C NMR spectra of 4–6% T-PDMS and 4–6% D-PDMS$_{2wt\%}$; Figure S17: Solution-Phase homonuclear ^{1}H-^{1}H correlation (COSY) spectrum of 4–6% T-PDMS; Figure S18: COSY spectrum of 4–6% T-PDMS$_{2wt\%}$; Figure S19: Amplitude sweeps of 13–17% T-PDMS and 13–17% D-PDMS$_{1wt\%}$; Figure S20: Amplitude sweeps of 4–6% T-PDMS, 4–6% D-PDMS$_{2wt\%}$, and 4–6% D-PDMS$_{6wt\%}$.; Figure S21: Percent increase in polymer mass (S%) of solid D-PDMS materials; Figure S22: TGA thermogram of 4–6% T-PDMS; Figure S23: TGA thermogram of 13–17% T-PDMS; Figure S24: TGA thermogram of 4–6% D-PDMS$_{2wt\%}$; Figure S25: TGA thermogram of 4–6% D-PDMS$_{6wt\%}$; Figure S26: TGA thermogram of 4–6% D-PDMS$_{55wt\%}$; Figure S27: TGA thermogram of 13–17% D-PDMS$_{6wt\%}$; Figure S28: TGA thermogram of 13–17% D-PDMS$_{15wt\%}$; Figure S29: TGA thermogram of 13–17% D-PDMS$_{55wt\%}$; Figure S30: TGA thermogram of 13–17% T-PDMS from the paired TGA-MS experiment; Figure S31: Mass spectrum of 13–17% T-PDMS from the paired TGA-MS experiment; Table S1: D-PDMS materials from reactions of 4–6% T-PDMS- and 13–17% T-PDMS at different initial and final concentrations; Table S2: Moles of thiol and dimethylsiloxane monomers per mole of T-PDMS; Table S3: Solvent Hildebrand solubility parameter (δ) and dielectric constant (ε), and swelling rankings *based on mass* (where 1 is best) for 4–6% D-PDMS$_{55wt\%}$ and other crosslinked PDMS materials. References cited: [27,36,46,47,55,57–60,66–72].

Author Contributions: Conceptualization, D.M.B. and R.G.W.; methodology, D.M.B. and R.G.W.; validation, D.M.B., R.G.W. and A.K.G.; formal analysis, D.M.B., R.G.W. and A.K.G.; resources, R.G.W. and A.K.G.; data curation, D.M.B., R.G.W. and A.K.G.; writing—original draft preparation, D.M.B., R.G.W. and A.K.G.; writing—review and editing, D.M.B., R.G.W. and A.K.G.; supervision, R.G.W.; project administration, R.G.W.; funding acquisition, R.G.W. All authors have read and agreed to the published version of the manuscript.

Funding: This research received funding through the US National Science Foundation (grant CHE-1502856) and Georgetown University.

Data Availability Statement: Not applicable.

Acknowledgments: We thank Louis Poon and Xinran Zhang for insightful discussions about results and concepts. We thank Prashant Pandey for assisting with obtaining the TGA-MS results.

Conflicts of Interest: The authors declare no conflict of interest.

References

1. Beaupre, D.M.; Weiss, R.G. Thiol- and Disulfide-Based Stimulus-Responsive Soft Materials and Self-Assembling Systems. *Molecules* **2021**, *26*, 3332. [CrossRef]
2. Jin, Y.; Yu, C.; Denman, R.J.; Zhang, W. Recent Advances in Dynamic Covalent Chemistry. *Chem. Soc. Rev.* **2013**, *42*, 6634–6654. [CrossRef]
3. Dutta, K.; Das, R.; Medeiros, J.; Thayumanavan, S. Disulfide Bridging Strategies in Viral and Nonviral Platforms for Nucleic Acid Delivery. *Biochemistry* **2021**, *60*, 966–990. [CrossRef]
4. Wang, Q.; Guan, J.; Wan, J.; Li, Z. Disulfide Based Prodrugs for Cancer Therapy. *RSC Adv.* **2020**, *10*, 24397–24409. [CrossRef]
5. Saito, G.; Swanson, J.A.; Lee, K.D. Drug Delivery Strategy Utilizing Conjugation via Reversible Disulfide Linkages: Role and Site of Cellular Reducing Activities. *Adv. Drug Deliv. Rev.* **2003**, *55*, 199–215. [CrossRef]
6. Leichner, C.; Jelkmann, M.; Bernkop-Schnürch, A. Thiolated Polymers: Bioinspired Polymers Utilizing One of the Most Important Bridging Structures in Nature. *Adv. Drug Deliv. Rev.* **2019**, *151–152*, 191–221. [CrossRef]
7. Yang, Y.; Urban, M.W. Self-Healing Polymeric Materials. *Chem. Soc. Rev.* **2013**, *42*, 7446–7467. [CrossRef]
8. Kim, S.M.; Jeon, H.; Shin, S.H.; Park, S.A.; Jegal, J.; Hwang, S.Y.; Oh, D.X.; Park, J. Superior Toughness and Fast Self-Healing at Room Temperature Engineered by Transparent Elastomers. *Adv. Mater.* **2018**, *30*, 1705145. [CrossRef]
9. Ling, L.; Li, J.; Zhang, G.; Sun, R.; Wong, C.P. Self-Healing and Shape Memory Linear Polyurethane Based on Disulfide Linkages with Excellent Mechanical Property. *Macromol. Res.* **2018**, *26*, 365–373. [CrossRef]
10. Zhang, X.; Han, L.; Liu, M.; Wang, K.; Tao, L.; Wan, Q.; Wei, Y. Recent Progress and Advances in Redox-Responsive Polymers as Controlled Delivery Nanoplatforms. *Mater. Chem. Front.* **2017**, *1*, 807–822. [CrossRef]
11. Zhuang, J.; Gordon, M.R.; Ventura, J.; Li, L.; Thayumanavan, S. Multi-Stimuli Responsive Macromolecules and Their Assemblies. *Chem. Soc. Rev.* **2013**, *42*, 7421–7435. [CrossRef]
12. Zhang, Z.P.; Rong, M.Z.; Zhang, M.Q. Polymer Engineering Based on Reversible Covalent Chemistry: A Promising Innovative Pathway towards New Materials and New Functionalities. *Prog. Polym. Sci.* **2018**, *80*, 39–93. [CrossRef]
13. Lv, C.; Zhao, K.; Zheng, J. A Highly Stretchable Self-Healing Poly(Dimethylsiloxane) Elastomer with Reprocessability and Degradability. *Macromol. Rapid Commun.* **2018**, *39*, 1700686. [CrossRef]
14. Tomei, M.R.; Cinti, S.; Interino, N.; Manovella, V.; Moscone, D.; Arduini, F. Paper-Based Electroanalytical Strip for User-Friendly Blood Glutathione Detection. *Sens. Actuator. B Chem.* **2019**, *294*, 291–297. [CrossRef]
15. Yin, W.; Ke, W.; Lu, N.; Wang, Y.Y.; Japir, A.A.W.M.M.; Mohammed, F.; Wang, Y.Y.; Pan, Y.; Ge, Z. Glutathione and Reactive Oxygen Species Dual-Responsive Block Copolymer Prodrugs for Boosting Tumor Site-Specific Drug Release and Enhanced Antitumor Efficacy. *Biomacromolecules* **2020**, *21*, 921–929. [CrossRef]
16. Gao, Y.; Dong, C.M. Reduction- and Thermo-Sensitive Core-Cross-Linked Polypeptide Hybrid Micelles for Triggered and Intracellular Drug Release. *Polym. Chem.* **2017**, *8*, 1223–1232. [CrossRef]
17. Utrera-Barrios, S.; Verdejo, R.; López-Manchado, M.A.; Hernández Santana, M. Evolution of Self-Healing Elastomers, from Extrinsic to Combined Intrinsic Mechanisms: A Review. *Mater. Horizons* **2020**, *7*, 2882–2902. [CrossRef]
18. Kolšek, K.; Aponte-Santamaría, C.; Gräter, F. Accessibility Explains Preferred Thiol-Disulfide Isomerization in a Protein Domain. *Sci. Rep.* **2017**, *7*, 9858. [CrossRef]
19. Patai, S. The Chemistry of the Thiol Group. In *The Chemistry of the Thiol Group: Patai's Chemistry of Functional Groups Vol. 2*; Wiley: London, UK, 1974; pp. 163–269.
20. Amamoto, Y.; Otsuka, H.; Takahara, A.; Matyjaszewski, K. Self-Healing of Covalently Cross-Linked Polymers by Reshuffling Thiuram Disulfide Moieties in Air under Visible Light. *Adv. Mater.* **2012**, *24*, 3975–3980. [CrossRef]
21. Parker, A.J.; Kharasch, N. The Scission Of The Sulfur-Sulfur Bond. *Chem. Rev.* **1959**, *59*, 583–628. [CrossRef]
22. Cremlyn, R.J. Thiols, Sulfides, and Sulfenic Acids. In *An Introduction to Organosulfur Chemistry*; Wiley: Chichester, UK, 1996; pp. 40–61.
23. Witt, D. Recent Developments in Disulfide Bond Formation. *Synthesis* **2008**, *16*, 2491–2509. [CrossRef]
24. Mandal, B.; Basu, B. Recent Advances in S-S Bond Formation. *RSC Adv.* **2014**, *4*, 13854–13881. [CrossRef]
25. Mekaru, H.; Yoshigoe, A.; Nakamura, M.; Doura, T.; Tamanoi, F. Biodegradability of Disulfide-Organosilica Nanoparticles Evaluated by Soft X-ray Photoelectron Spectroscopy: Cancer Therapy Implications. *ACS Appl. Nano Mater.* **2019**, *2*, 479–488. [CrossRef]
26. Doura, T.; Nishio, T.; Tamanoi, F.; Nakamura, M. Relationship between the Glutathione-Responsive Degradability of Thiol-Organosilica Nanoparticles and the Chemical Structures. *J. Mater. Res.* **2019**, *34*, 1266–1278. [CrossRef]
27. Yu, T.; Wakuda, K.; Blair, D.L.; Weiss, R.G. Reversibly Cross-Linking Amino-Polysiloxanes by Simple Triatomic Molecules. Facile Methods for Tuning Thermal, Rheological, and Adhesive Properties. *J. Phys. Chem. C* **2009**, *113*, 11546–11553. [CrossRef]
28. Liu, J.; Yao, Y.; Li, X.; Zhang, Z. Fabrication of Advanced Polydimethylsiloxane-Based Functional Materials: Bulk Modifications and Surface Functionalizations. *Chem. Eng. J.* **2021**, *408*, 127262. [CrossRef]
29. De Keer, L.; Kilic, K.I.; Van Steenberge, P.H.M.; Daelemans, L.; Kodura, D.; Frisch, H.; De Clerck, K.; Reyniers, M.F.; Barner-Kowollik, C.; Dauskardt, R.H.; et al. Computational Prediction of the Molecular Configuration of Three-Dimensional Network Polymers. *Nat. Mater.* **2021**, *20*, 1422–1430. [CrossRef]

30. Quake, S.R.; Scherer, A. From Micro- to Nanofabrication with Soft Materials. *Science* **2000**, *290*, 1536–1540. [CrossRef]
31. Rus, D.; Tolley, M.T. Design, Fabrication and Control of Soft Robots. *Nature* **2015**, *521*, 467–475. [CrossRef]
32. Eduok, U.; Faye, O.; Szpunar, J. Recent Developments and Applications of Protective Silicone Coatings: A Review of PDMS Functional Materials. *Prog. Org. Coatings* **2017**, *111*, 124–163. [CrossRef]
33. Partenhauser, A.; Laffleur, F.; Rohrer, J.; Bernkop-Schnürch, A. Thiolated Silicone Oil: Synthesis, Gelling and Mucoadhesive Properties. *Acta Biomater.* **2015**, *16*, 169–177. [CrossRef]
34. Partenhauser, A.; Netsomboon, K.; Leonaviciute, G.; Bernkop-Schnürch, A. Evaluation of Thiolated Silicone Oil as Advanced Mucoadhesive Antifoaming Agent. *Drug Deliv.* **2016**, *23*, 2711–2719. [CrossRef]
35. Fürst, A.; Baus, R.A.; Lupo, N.; Bernkop-Schnürch, A. Entirely S-Protected Thiolated Silicone: A Novel Hydrophobic Mucoadhesive and Skin Adhesive. *J. Pharm. Sci.* **2019**, *108*, 2887–2894. [CrossRef]
36. Grießinger, J.A.; Bonengel, S.; Partenhauser, A.; Ijaz, M.; Bernkop-Schnürch, A. Thiolated Polymers: Evaluation of Their Potential as Dermoadhesive Excipients. *Drug Dev. Ind. Pharm.* **2017**, *43*, 204–212. [CrossRef] [PubMed]
37. Kulawik-Pióro, A.; Drabczyk, A.K.; Kruk, J.; Wróblewska, M.; Winnicka, K.; Tchórzewska, J. Thiolated Silicone Oils as New Components of Protective Creams in the Prevention of Skin Diseases. *Materials* **2021**, *14*, 4723. [CrossRef]
38. Wei, C.; Chen, M.; Liu, D.; Zhou, W.; Khan, M.; Wu, X.; Huang, N.; Li, L. A Recyclable Disulfide Bond Chemically Cross-Linking, High Toughness, High Conductivity Ion Gel Based on Re-Shaping and Restructuring in the Gel State. *Polym. Chem.* **2015**, *6*, 4067–4070. [CrossRef]
39. Wei, C.; Chen, M.; Liu, D.; Zhou, W.; Khan, M.; Wu, X.; Huang, N.; Li, L. Synthesis of Recyclable, Chemically Cross-Linked, High Toughness, High Conductivity Ion Gels by Sequential Triblock Copolymer Self-Assembly and Disulfide Bond Cross-Linking. *RSC Adv.* **2015**, *5*, 22638–22646. [CrossRef]
40. Naga, N.; Moriyama, K.; Furukawa, H. Synthesis and Properties of Multifunctional Thiol Crosslinked Gels Containing Disulfide Bond in the Network Structure. *J. Polym. Sci. Part A Polym. Chem.* **2017**, *55*, 3749–3756. [CrossRef]
41. Colby, R.H. Structure and Linear Viscoelasticity of Flexible Polymer Solutions: Comparison of Polyelectrolyte and Neutral Polymer Solutions. *Rheol. Acta* **2010**, *49*, 425–442. [CrossRef]
42. Pomposo, J.A.; Perez-Baena, I.; Lo Verso, F.; Moreno, A.J.; Arbe, A.; Colmenero, J. How Far Are Single-Chain Polymer Nanoparticles in Solution from the Globular State? *ACS Macro Lett.* **2014**, *3*, 767–772. [CrossRef]
43. Mavila, S.; Eivgi, O.; Berkovich, I.; Lemcoff, N.G. Intramolecular Cross-Linking Methodologies for the Synthesis of Polymer Nanoparticles. *Chem. Rev.* **2016**, *116*, 878–961. [CrossRef] [PubMed]
44. Prasher, A.; Loynd, C.M.; Tuten, B.T.; Frank, P.G.; Chao, D.; Berda, E.B. Efficient Fabrication of Polymer Nanoparticles via Sonogashira Cross-Linking of Linear Polymers in Dilute Solution. *J. Polym. Sci. Part A Polym. Chem.* **2016**, *54*, 209–217. [CrossRef]
45. Bae, S.; Galant, O.; Diesendruck, C.E.; Silberstein, M.N. The Effect of Intrachain Cross-Linking on the Thermomechanical Behavior of Bulk Polymers Assembled Solely from Single Chain Polymer Nanoparticles. *Macromolecules* **2018**, *51*, 7160–7168. [CrossRef]
46. Gelest, Inc. *SMS-042-[4-6% (mercaptopropyl)methylsiloxane]-dimethylsiloxane Copoloymer*; SDS No. SMS-042; Gelest, Inc.: Morrisville, PA, USA, 2015.
47. Gelest, Inc. *SMS-142-[13-17% (mercaptopropyl)methylsiloxane]-dimethylsiloxane Copolymer*; SDS No. SMS-142; Gelest, Inc.: Morrisville, PA, USA, 2017.
48. Gottlieb, H.E.; Kotlyar, V.; Nudelman, A. NMR Chemical Shifts of Common Laboratory Solvents as Trace Impurities. *J. Org. Chem.* **1997**, *62*, 7512–7515. [CrossRef]
49. Morcombe, C.R.; Zilm, K.W. Chemical Shift Referencing in MAS Solid State NMR. *J. Magn. Reson.* **2003**, *162*, 479–486. [CrossRef]
50. Nieuwendall, R.C. How to Measure Absolute P3HT Crystallinity via CPMAS NMR. *Mag. Reson. Chem.* **2016**, *54*, 740–747. [CrossRef]
51. Kuhn, W.; Balmer, G. Crosslinking of Single Linear Macromolecules. *J. Polym. Sci.* **1962**, *57*, 311–319. [CrossRef]
52. Bourlès, E.; Alves de Sousa, R.; Galardon, E.; Selkti, M.; Tomas, A.; Artaud, I. Synthesis of Cyclic Mono- and Bis-Disulfides and Their Selective Conversion to Mono- and Bis-Thiosulfinates. *Tetrahedron* **2007**, *63*, 2466–2471. [CrossRef]
53. Lepucki, P.; Dioguardi, A.P.; Karnaushenko, D.; Schmidt, O.G.; Grafe, H.J. The Normalized Limit of Detection in NMR Spectroscopy. *J. Magn. Reson.* **2021**, *332*, 107077. [CrossRef]
54. Samoson, A.; Tuherm, T.; Past, J.; Reinhold, A.; Anupold, T.; Heinmaa, I. New Horizons for Magic-Angle Spinning NMR. In *New Techniques in Solid State NMR. Topics in Current Chemistry*; Klinowski, J., Ed.; Springer: Berlin/Heidelberg, Germany, 2005; Volume 246, pp. 15–31.
55. Lee, J.N.; Park, C.; Whitesides, G.M. Solvent Compatibility of Poly(Dimethylsiloxane)-Based Microfluidic Devices. *Anal. Chem.* **2003**, *75*, 6544–6554. [CrossRef]
56. Yilgor, I.; Eynur, T.; Yilgor, E.; Wilkes, G.L. Contribution of Soft Segment Entanglement on the Tensile Properties of Silicone-Urea Copolymers with Low Hard Segment Contents. *Polymer* **2009**, *50*, 4432–4437. [CrossRef]
57. Brennan, D.P.; Dobley, A.; Sideris, P.J.; Oliver, S.R.J. Swollen Poly(Dimethylsiloxane) (PDMS) as a Template for Inorganic Morphologies. *Langmuir* **2005**, *21*, 11994–11998. [CrossRef] [PubMed]
58. Favre, E. Swelling of Crosslinked Polydimethylsiloxane Networks by Pure Solvents: Influence of Temperature. *Eur. Polym. J.* **1996**, *32*, 1183–1188. [CrossRef]

59. Iagatti, A.; Patrizi, B.; Basagni, A.; Marcelli, A.; Alessi, A.; Zanardi, S.; Fusco, R.; Salvalaggio, M.; Bussotti, L.; Foggi, P. Photophysical Properties and Excited State Dynamics of 4,7-Dithien-2-Yl-2,1,3-Benzothiadiazole. *Phys. Chem. Chem. Phys.* **2017**, *19*, 13604–13613. [CrossRef]
60. Mao, H.; Qiu, Z.; Xie, B.; Wang, Z.; Shen, Z.; Hou, W. Development and Application of Ultra-High Temperature Drilling Fluids in Offshore Oilfield around Bohai Sea Bay Basin, China. *Offshore Technol. Conf. Asia 2016, OTCA 2016* **2016**, *March*, 1201–1222. [CrossRef]
61. Mallia, V.A.; Blair, D.L.; Weiss, R.G. Oscillatory Rheology and Surface Water Wave Effects on Crude Oil and Corn Oil Gels with (R)-12-Hydroxystearic Acid as Gelator. *Ind. Eng. Chem. Res.* **2016**, *55*, 954–960. [CrossRef]
62. Vandeputte, A.G.; Reyniers, M.F.; Marin, G.B. Theoretical Study of the Thermal Decomposition of Dimethyl Disulfide. *J. Phys. Chem. A* **2010**, *114*, 10531–10549. [CrossRef]
63. Sehon, A.H.; Darwent, B.D. The Thermal Decomposition of Mercaptans. *J. Am. Chem. Soc.* **1954**, *76*, 4806–4810. [CrossRef]
64. Yao, Q.; Wilkie, C.A. How Does Cross-Linking Affect the Thermal Stability of Polyisoprene? *Polym. Degrad. Stab.* **2000**, *69*, 287–296. [CrossRef]
65. Faragher, W.F.; Morrell, J.C.; Comay, S. Thermal Decomposition of Organic Sulfur Compounds. *Ind. Eng. Chem.* **1928**, *20*, 527–532. [CrossRef]
66. Voronkov, M.G.; Klyuchnikov, V.A.; Mironenko, E.V.; Shvets, G.N.; Danilova, T.F.; Khudobin, Y.I. Thermochemistry of Organosilicon Compounds: V. Thermochemical Properties of Perorganyloligocyclosiloxanes. *J. Organomet. Chem.* **1991**, *406*, 91–97. [CrossRef]
67. Advamacs.com Boiling Point Calculator. Available online: http://www.trimen.pl/witek/calculators/wrzenie.html (accessed on 10 March 2022).
68. SDBSWeb. Available online: https://sdbs.db.aist.go.jp/sdbs/cgi-bin/direct_frame_top.cgi (accessed on 26 October 2022).
69. Kleinberg, J.; Davidson, A.W. The Nature of Iodine Solutions. *Chem. Rev.* **1948**, *42*, 601–609. [CrossRef] [PubMed]
70. Winther, J.R.; Thorpe, C. Quantification of Thiols and Disulfides. *Biochim. Biophys. Acta-Gen. Subj.* **2014**, *1840*, 838–846. [CrossRef] [PubMed]
71. Jordan, F.; Hoops, P.; Kudzin, Z.; Kudzin, Z.; Witczak, Z. Nuclear Magnetic Resonance Determination of the Site of Acylation of the Tautomeric Nucleophile 4-Thioxopyridine. *J. Org. Chem.* **1986**, *51*, 571–573. [CrossRef]
72. Egwim, I.O.C.; Gruber, H.J. Spectrophotometric Measurement of Mercaptans with 4,4′-Dithiodipyridine. *Anal. Biochem.* **2001**, *288*, 188–194. [CrossRef] [PubMed]